Quantum Electronics **48** (7) 630–636 (2018) ©2018 Kvantovaya Elektronika and Turpion Ltd

NANOSTRUCTURES https://doi.org/10.1070/QEL16622

Simulation of the optical properties of surface nanostructures for photoacoustic converters

A.P. Mikitchuk, K.V. Kozadaev

Abstract. **A computer model has been developed and a theoretical study has been performed for nanostructures in the form of a two-dimensional monolayer of nanoparticles of noble metals on an optical fibre end face. The parameters of nanostructure-based photoacoustic converters are chosen for different environments in order to provide a high light absorption coefficient, which, in turn, provides a maximally high conversion efficiency for ultrasound generation. It is established that efficient photoacoustic conversion can be implemented in a surface nanostructure composed of spherical gold nanoparticles, located on an optical fibre end face in water, in wide ranges of the nanostructure microscopic parameters. It is shown that the backscattering coefficient also turns out large in the case of resonance absorption; for this reason, one must provide optical isolation of a laser in use when designing photoacoustic generators.**

Keywords: *photoacoustic generation, surface nanostructure, metal nanoparticle monolayer, optical fibre, surface plasmon resonance, electromagnetic simulation.*

1. Introduction

The intensification of studies in the field of photoacoustic ultrasonic generation is due to the wide range of possible applications of broadband ultrasonic generators for diagnostics of different media [1–5]. For example, the biological and medical applications are related to the necessity of high-resolution imaging in endoscopic, intravascular, and ophthalmologic studies [1, 6] and in the analysis of proteins and cells under laboratory conditions [7, 8]. No less important are the commercial applications of these generators for nondestructive control of defects in parts and for monitoring of complex soldered units [9–12]. Generation of broadband ultrasonic signals can be observed when irradiating thin absorbing media by a high-power modulated laser beam [13]. The irradiation provides expansion–compression cycles for a photoacoustic material, which generate acoustic waves in the converter environment. The uniformity of the front of the formed acoustic wave depends strongly on the absorbing-layer thickness; as a result, in most of practical photoacoustic applications, it is necessary to provide absorption of an incident laser beam in a maximally thin layer of the photoacoustic converter.

A.P. Mikitchuk, K.V. Kozadaev Belarusian State University, prosp. Nezavisimosti 4, 220030 Minsk, Belarus; e-mail: m.helenay@yandex.by

Received 4 February 2018; revision received 9 April 2018
Kvantovaya Elektronika **48** (7) 630–636 (2018)
Translated by Yu.P. Sin'kov

A promising direction in the design of ultrasonic generators is the development of fibre-optic photoacoustic converters, which have a number of advantages: compact sizes (several hundreds of micrometers), small weight (several tenths of gram), immunity to electromagnetic interference, wide frequency bandwidth, dielectric version, mechanical flexibility, and high chemical durability [13]. A no less important parameter is the beam quality at the fibre output (the parameter M^2, factor of proximity of the optical power spatial distribution in the laser beam to Gaussian, should be close to unity). The latter condition can be implemented for a single-mode optical fibre with an ultrapolished end face, oriented strictly perpendicular to the fibre axis (modern optical fibres with a W-shaped refractive index profile provide a beam quality at the fibre output at a level of $M^2 < 1.02$) [14].

To minimise the thickness of the photoacoustic material layer in fibre-optic ultrasonic converters, surface nanostructures in the form of two-dimensional arrays of noble metal nanoparticles can be used as an absorbing medium [13]. These nanostructures have a very large aspect ratio (the ratio of longitudinal sizes to thickness) and fairly high photostability (illumination does not lead to degradation of nanoparticle absorbing layer). The necessary absorption coefficient at the wavelength of incident laser beam is obtained due to the effect of surface plasmon resonance (SPR) [13]. Such structures can be synthesised from nanoparticles of noble metals (Ag, Au, Pt, Pd) by chemical vapour deposition, optical arrangement [15], vacuum deposition [16], or atmospheric laser deposition [17, 18].

These structures are used as a rule in liquid media, e.g., in water or biological fluids, because an ultrasonic signal propagating in a liquid is attenuated much more slowly than that in air [13]. Various polymers are generally applied to form a mechanical protective layer for nanoparticles on a fibre [2–5]. However, when a solid sample under study cannot be placed in a liquid, an ultrasonic converter is brought into contact with the solid so as to minimise the air gap between them [9].

When searching for optimal nanostructures for photoacoustic converters, the fabrication of experimental samples is a rather expensive and long-term procedure. The choice of desired parameters of the nanostructured working surface of a fibre end face can be significantly simplified by means of computer simulation of its optical properties [19, 20]. The purpose of this work was to develop a computer model and perform a theoretical analysis of nanostructures in the form of a two-dimensional monolayer of noble metal nanoparticles on a fibre end face, as well as to choose appropriate parameters of nanostructure-based photoacoustic converters for different environments in order to implement a high light

absorption coefficient, which, in turn, provides the most efficient generation of ultrasound.

2. Computer simulation of surface nanostructures and convergence of simulation methods

Figure 1 shows the schematic of the photoacoustic converter. The converter consists of a substrate (fibre end face) with a surface array of monodispersive metal nanoparticles in an environment (the latter was considered to be air or water). Its simulation was performed by means of CST Microwave Studio SE software. The simulation was performed for uniform excitation of nanostructures by light, which is approximately valid for the mode spot centre in the case of a single-mode optical fibre (calculations were performed for single-mode visible-light fibres; examples are Corning RGB 400 or FibreCore SM450). Note that the program package applied here was historically developed as a tool for simulating microwave structures and antennas [21]. For this reason, the computational algorithms are optimised to calculate the scattering matrices (*S*-parameters), which relate the incident and reflected electromagnetic waves in an arbitrary complex network [22].

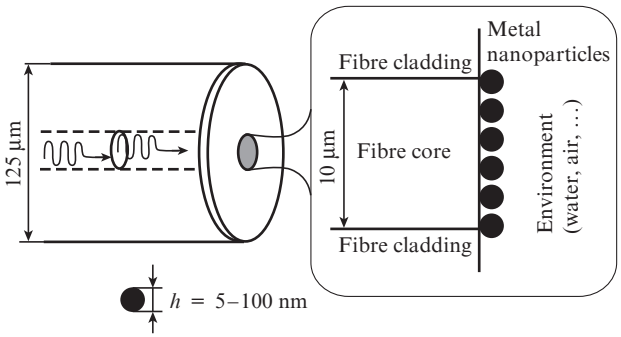

Figure 1. Schematic of the nanostructure: metal nanoparticles are deposited on the surface of a substrate (single-mode optical fibre); the sizes of the fibre core and spherical nanoparticles are indicated.

The model unit cell of minimum size, corresponding to a single lattice point of a structure with translational symmetry in two dimensions, consists of two contacting parallelepipeds. One is formed by the substrate material and the other contains nanoparticles and environment (Fig. 2). The nanoparticles are located on the interface between the parallelepipeds. Nanoparticles bases are placed on the substrate surface. The semi-infinite (in the direction normal to the interface) substrate and environment layers are modelled using absorbing boundary conditions, implemented via Floquet ports. These ports in the CST Microwave Studio SE package are ideally matched layers (there are several layers of additional cells, located beyond the modelled volume; the fields in these cells are calculated with allowance for the large virtual loss) [23, 24].

A planar structure translation to infinity along the x and y axes is implemented using boundary unit-cell conditions. Thus, using the finite integral technique (implemented in the CST Microwave Studio SE package), one can take into account the collective interactions in the entire system: nanoparticles – neighbouring nanoparticles – substrate – environment. A complete electromagnetic simulation of the structure [25] is performed in the following way. Note that the use of boundary conditions for a unit cell allows one (in the general case) to take into account the multipole interaction in the ensemble of periodically spaced nanoparticles.

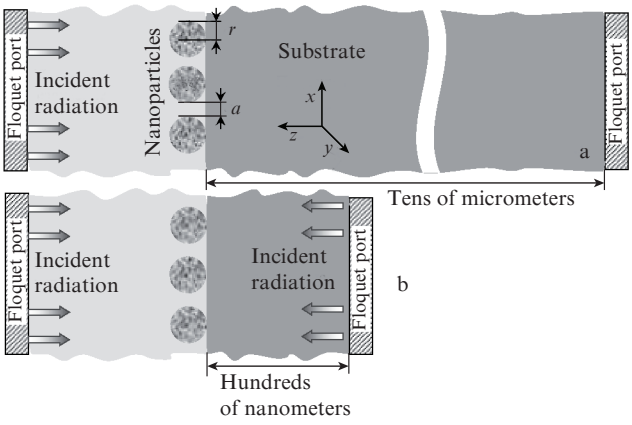

Figure 2. Simulation schemes for surface nanostructures with metal nanoparticles on a substrate in an environment (air, water), which are based on (a) analysing the electromagnetic field in the far-field zone and (b) recalculating the *S*-matrices. The unit cell is shown in the xz and yz planes.

Calculations are performed with a tetrahedral spatial mesh, which yields most accurate results under specified unit-cell boundary conditions [20, 25, 26]. Iterative simulations should be performed in order to reduce the influence of spatial mesh parameters for every nanostructure type. Such iterations are carried out until simulation results get steady state values.

In a number of previous papers, we applied an analysis of the electromagnetic far-field by means of CST Microwave Studio SE [19, 20, 25]. Electromagnetic field simulation shows that a stationary periodic distribution of the electromagnetic field is formed rather rapidly in the substrate [25, 27]. This effect was observed even when domains of anomalously strong electric field manifested themselves; these domains are indicative of intense resonance collective interaction between nanoparticles in the layer [25]. To make the computer simulation more efficient, we propose to use the electromagnetic field characteristics calculated with the help of the *S*-matrices. Moreover, the simulation of nanostructures with smaller substate is proposed. This allows one to significantly reduce the number of sampling cells for the structure (Fig. 2b). Spectral dependences of the light absorption coefficient, which is determined by the radiation energy dissipation in the modelled structure, were calculated.

The system of universal *S*-parameters makes it possible to relate the incident and reflected waves in an arbitrary complex network. The relation between the *S*-parameters and the amplitudes of incident ($a_{1,2}$) and reflected ($b_{1,2}$) waves is given by the expression [22]

$$\begin{pmatrix} b_1 \\ b_2 \end{pmatrix} = \begin{pmatrix} S_{11} & S_{21} \\ S_{12} & S_{22} \end{pmatrix} \begin{pmatrix} a_1 \\ a_2 \end{pmatrix},$$

where S_{11} is the reflectance from the substrate to the substrate, S_{12} is the transmittance from the environment to the substrate, S_{21} is the transmittance from the substrate to the

nanoparticle layer, and S_{22} is the reflectance from the nanoparticle layer to the environment.

Figure 3 shows how the S-matrix components are determined at some frequency, when radiation is incident on the structure from two sides: from the nanoparticle layer and from the substrate (fibre end face).

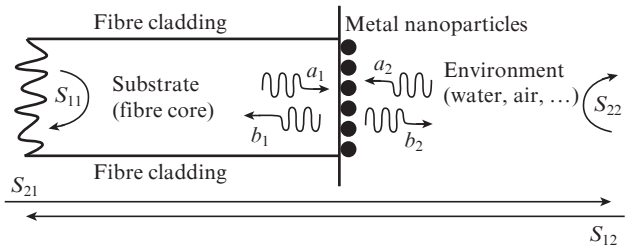

Figure 3. Determination of the S-matrix components at some frequency, when the structure is irradiated from two sides: from the side of the nanoparticles and from the side of the substrate (optical fibre); a_1 and a_2 are the complex amplitudes of the waves incident on the nanostructure and b_1 and b_2 are the complex amplitude of the waves reflected from it.

On the assumption that laser radiation illuminates the nanostructure from only the fibre, the extinction coefficient is calculated at each wavelength using the relation

$$k = S_{11} + (1 - S_{21} - S_{11}) = 1 - S_{21}.$$

In turn, the absorption coefficient is calculated from the formula

$$l = 1 - S_{21} - S_{11}.$$

The input data for a computer model are the type of material, shape, and sizes of nanoparticles; the types of substrate material and environment; and the incident radiation parameters. Note that the dispersion of the optical constants of metals is taken into account by interpolating the spectral data of [28].

The surface occupation density is equal to the ratio of the area of nanoparticle projection onto the substrate, S_{NP}, to the unit cell-base area S_{UC}. For example, the surface occupation density for spherical nanoparticles can be determined as

$$\rho = \frac{S_{NP}}{S_{UC}} = \frac{\pi r^2}{l^2} = \frac{\pi r^2}{(2r + ar)^2} = \frac{\pi}{(2 + a)^2},$$

where a is the distance between the projections of nanoparticles onto the substrate, expressed in terms of their radius r [20].

Figure 4 shows the results of simulating the extinction efficiency based on the far-field analysis (dots) and based on S-matrices (solid curves) for spherical, conical, and pyramidal (with an octagonal base) silver nanoparticles on a substrate (the end face of a fibre with a refractive index $n \approx 1.46$) in air (the refractive index $n_{air} \approx 1$). The parameters were as follows: the nanoparticle base radius $r = 25$ nm, the nanoparticle height $h = 2r = 50$ nm, and the surface occupation density $\rho = 46\%$. During far-field simulation, the software package automatically sets reference wavelengths (from a specified wavelength range), for which the optical characteristics of the nanostructure are calculated. A new (different from the previous) sequence of reference wavelengths is automatically formed for each value of the sweep parameter; these wavelengths may differ from the real wavelength corresponding to the maximum in the absorption spectrum. To reduce the influence of this effect on simulation results, one must increase the computational mesh density. As a result, the calculation time for each reported absorption spectrum significantly increases. Thus, the far-field analysis is not always efficient: first, simulation results may depend strongly on the computational grid parameters and, second, an excess sampling of the structure studied is often called for.

The convergence of simulation can be studied by analysing the relative residual uncertainty (residual). The residuals in the range from 10^{-13} to 10^{-12} are obtained for all the wave-

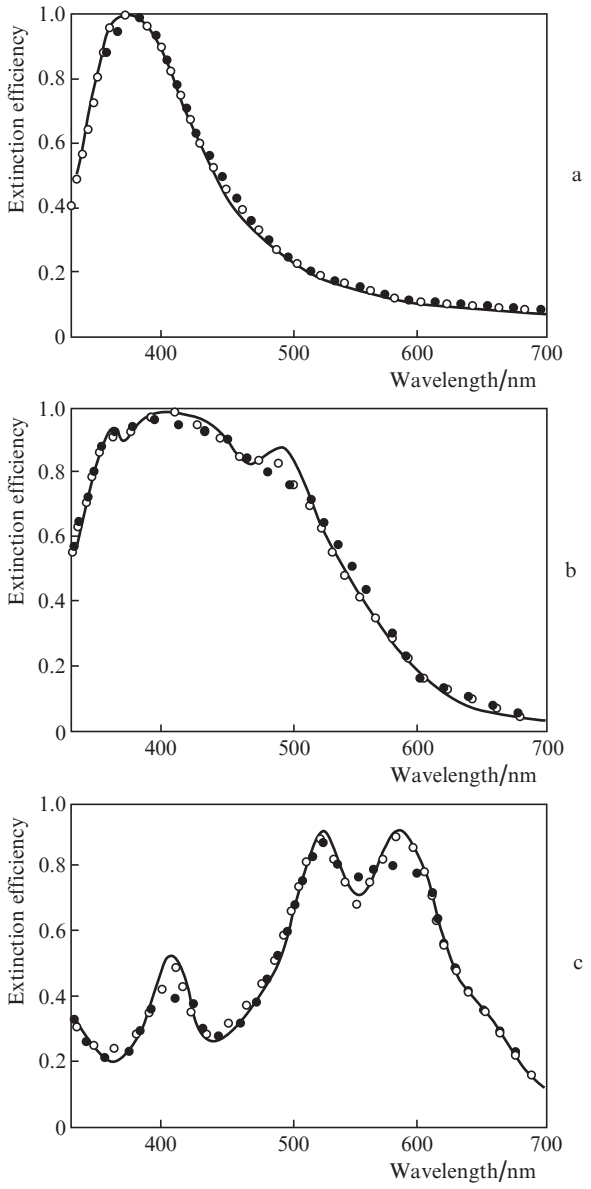

Figure 4. Results of simulating the extinction efficiency based on the analysis of electromagnetic field in the far-field zone (circles) and on the S matrices (solid lines) for (a) spherical, (b) conical, and (c) pyramidal (with an octagonal base) silver nanoparticles deposited on a substrate. The filled and open circles correspond to 25 and 35 lines per wavelength, respectively.

lengths under study. At the same time, the specified maximum residual value was set to be 10^{-12}. Near the SPR peak, the residual strongly oscillates due to the resonant distribution of the electromagnetic field.

3. Optical characteristics of surface nanostructures with metal nanoparticles for fibre-optic photoacoustic converters

The absorption spectrum was simulated in the wavelength range of 330–850 nm, where the light absorption coefficient of gold and silver nanoparticles of most typical shapes is maximal [29]. For example, the SPR peak for spherical silver and gold nanoparticles lies in the wavelength range of 330–550 nm. Hence, in designing photoacoustic generators, one can use commercially available solid-state frequency-conversion lasers (wavelength of 532 nm) and direct-generation semiconductor lasers (wavelengths in the range of 510–530 nm and wavelengths of 405, 445, and 450 nm) [30].

The possibility of efficient photoacoustic conversion is determined by a set of factors (e.g., the thermophysical and hydrodynamic properties of nanostructure), whose consideration is beyond the scope of this study. To implement an efficient (from the point of view of high modulated light absorption in the nanostructure) photoacoustic transformation, it is necessary to satisfy several conditions simultaneously:

1. Availability of a laser generating modulated radiation in the desired wavelength range.

2. A sufficiently wide SPR peak (with a width more than 25 nm at a level of 0.9) to provide a possibility of wavelength multiplexing for different lasers.

3. High absorption coefficient in the SPR peak (50% or more).

Note that in this case it is not quite correct to introduce the photoacoustic conversion efficiency as a numerical value, because some conditions do not allow for clear mathematical formulation.

Figure 5 shows the SPR peak positions in the absorption spectrum of the nanostructure with gold nanoparticles on a fibre end face in water, depending on the nanoparticle radius and the surface occupation density (fibre end face). The domain of existence of commercially available lasers providing generation of modulated optical signal is shown grey.

Figure 6 presents the SPR peak width at a level of 0.9 in the absorption spectrum of the nanostructure with spherical gold nanoparticles on a fibre end face in water, depending on the nanoparticle radius and the surface occupation density. It can be seen that the range where the SPR peak width at a level of 0.9 exceeds 25 nm covers almost the entire range of the simulated parameters, except for a small interval, extending from the point corresponding to the surface occupation density $\rho = 55\%$ and nanoparticle radius $r = 2.5$ nm to the point with $\rho = 35\%$ and $r = 13$ nm.

Figure 7 shows the absorption coefficients within the SPR peak in the absorption spectrum of the nanostructure with spherical gold nanoparticles in water as functions of the nanoparticle radius and the surface occupation density. It can be seen that there is an extended interval in which the absorption coefficient in the SPR peak exceeds 49%. The domain where all three conditions necessary for efficient photoacoustic conversion are satisfied is outlined by a contour. It is important that, in the case of particles with radii of 18–23 nm, a change in the surface occupation density in the range of

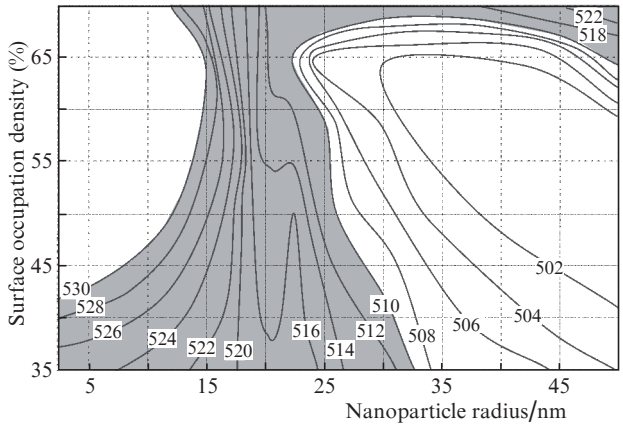

Figure 5. Positions of the SPR peak in the absorption spectrum of the nanostructure with spherical gold nanoparticles on a fibre end face in water, depending on the nanoparticle radius and the surface occupation density. The domain of existence of commercially available lasers, providing generation of a modulated optical signal, is shown grey. The numbers on the curves indicate the SPR peak positions in nm.

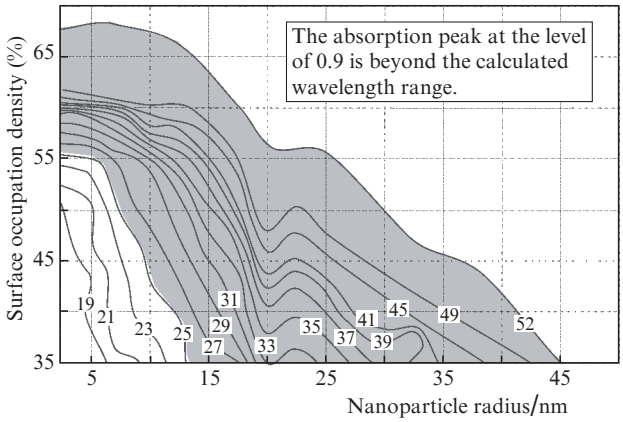

Figure 6. SPR peak widths at the level of 0.9 in the absorption spectrum of a nanostructure with spherical gold nanoparticles on a fibre end face in water, depending on the nanoparticle radius and the surface occupation density. The region where the SPR peak width exceeds 25 nm is shown grey. The numbers on the curves indicate the SPR peak widths in nm.

35%–70% does not affect much the photoacoustic conversion efficiency.

Figure 8 shows the absorption coefficients within the SPR peak in the absorption spectrum of the same nanostructure but with air environment. In the case of a nanostructure with silver nanoparticles formed on a fibre end face and located in air, the domain where all three conditions necessary for efficient photoacoustic conversion are satisfied is very small: the nanoparticle radii and the surface occupation densities range from 8 to 15 nm and from 57% to 62%, respectively.

There are some peculiarities in the spectral behaivour of the SPR peak for gold nanoparticles on the fiber end face in water (Figs 5–7) with any surface occupation densities and sizes in the range of 18–24 nm. A simulation of the spatial distribution of the electric field strength (field distributions in the same phase were compared) in the nanostructure, both at a wavelength near the SPR peak and directly at the absorption peak, revealed the following. In the case of small

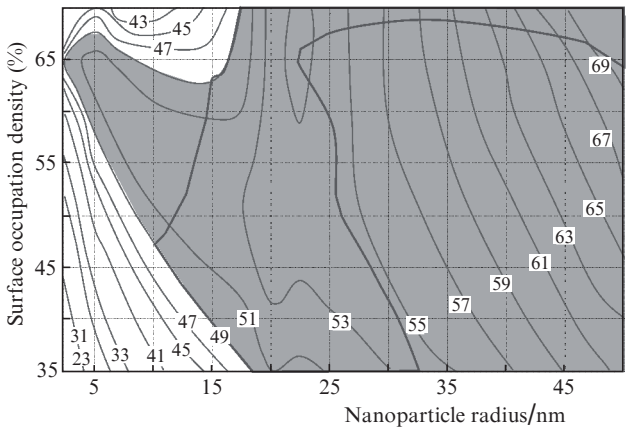

Figure 7. Absorption coefficients within the SPR peak in the absorption spectrum of the nanostructure with spherical gold nanoparticles on a fibre end face in water, depending on the nanoparticle radius and the surface occupation density. The region where the absorption coefficient in the peak exceeds 49% is shown grey. The domain in which all three necessary conditions for efficient photoacoustic conversion are satisfied is outlined by a contour. The numbers on the curves are absorption coefficients in percent.

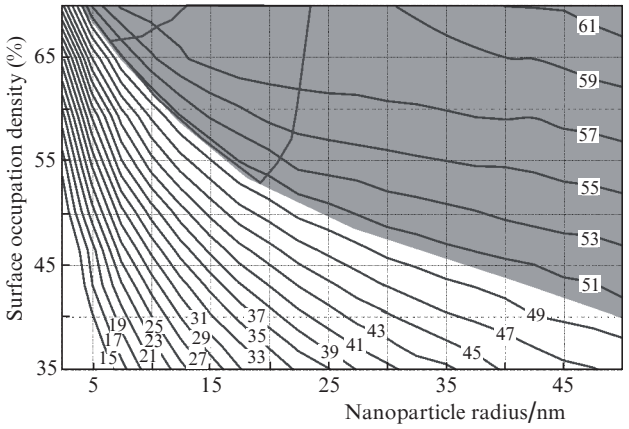

Figure 8. Absorption coefficients within the SPR peak in the absorption spectrum of the nanostructure with spherical gold nanoparticles on a fibre end face in air, depending on the nanoparticle radius and the surface occupation density. The region where the absorption coefficient in the peak exceeds 50% is shown grey. The domain in which all three necessary conditions for efficient photoacoustic conversion are satisfied is outlined by a contour. The numbers on the curves are absorption coefficients in percent.

nanoparticles (whose sizes are comparable with the penetration depth of the perturbed electromagnetic field into the substrate), the field in the nanoparticles–surrounding water–substrate system oscillates as a single whole. A coupled system of collective electron plasma and electromagnetic field is formed. Here, the perturbed substrate field affects significantly the nanoparticles. For large nanoparticles (whose sizes exceed the penetration depth of the perturbed electromagnetic field into the substrate), the fraction of the energy of the perturbed electromagnetic field concentrated in the substrate is small in comparison with the energy in the nanoparticles–environment system. The region with pecularities of the SPR-peak bahaivour is a transition region from the coupled system of electron plasma and electromagnetic field of the whole structure to the oscillating nanoparticles–environment system. Note that the permittivity of environment affects much the spatial distribution of electric field strength: in the case of air, the perturbed field penetrates at a large depth into the medium surrounding nanoparticles. For this reason, the transition region is absent in Fig. 8.

When designing photoacoustic converters, it is also important to take into account the magnitude of the back-reflection from the nanostructure, because this effect may disturb the generation of a semiconductor laser. Figure 9 shows wavelength dependences of the absorption coefficient and the back-reflectance to the fibre for a nanostructure with spherical gold nanoparticles on the fibre end face in air for different surface occupation densities. It can be seen that, for the parameters providing a maximum light absorption in the nanostructure, the back-reflectance to the optical fibre may be rather high (up to –3 dB) at a surface occupation density of about 70%. A decrease in surface occupation density results in decreasing of back-reflectance. The back-reflection reaches a maximum at the wavelengths corresponding to the maxima of SPR peaks and sharply decreases at both sides of these peaks; this decrease is more pronounced on the short-wavelength side as compared with the long-wavelength one. When designing photoacoustic generators, one must isolate a laser (using, e.g., a fibre-optic isolator) in order to preven back-reflection to the laser cavity.

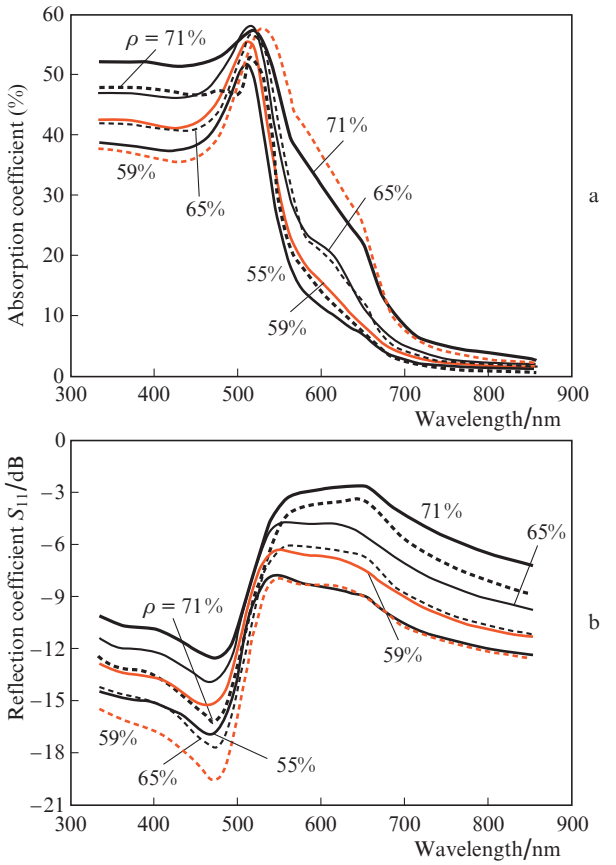

Figure 9. Wavelength dependences of the (a) absorption and (b) reflection coefficients in the case of a nanostructure with spherical gold nanoparticles on a fibre end face in air, for different surface occupation densities ρ and particle radii of 15 (dashed lines) and 20 (solid lines) nm.

Note that the absorption coefficient is affected by many factors (e.g., nanoparticle material and the refractive indices of the fibre core and nanoparticle environment). Figure 10 shows absorbtion coefficient versus wavelength for nanostructures with spherical gold and silver nanoparticles (with a radius of 20 nm and a surface occupation density of 46%) on a fibre end face for different refractive indices of the nanoparticle environment. It can be seen that, with an increase in the refractive index of environment, the maximum of the SPR peak for these two types of nanostructures becomes red-shifted. In the wavelength range of 490–650 nm for the nanostructures with gold nanoparticles, the position of the SPR peak changes by ~50 nm with a change in the refractive index by unity (Fig. 10a), whereas in the range of 370–590 nm for the nanostructures with silver nanoparticles it changes by ~110 nm with the same change in the refractive index (Fig. 10b). It can also be seen that, when the refractive indices of the environment and substrate are identical, the absorption spectra contains one maximum, whereas an increase in the refractive index of the environment gives rise to the second maximum in the spectrum. This is likely due to the difference in the interaction between excited plasmonic oscillations for different systems: nanoparticles and substrate. As the simulation shows, the penetration depth into the substrate for the electromagnetic field perturbed by plasmon resonance exceeds that for the environment of nanoparticles [20, 27].

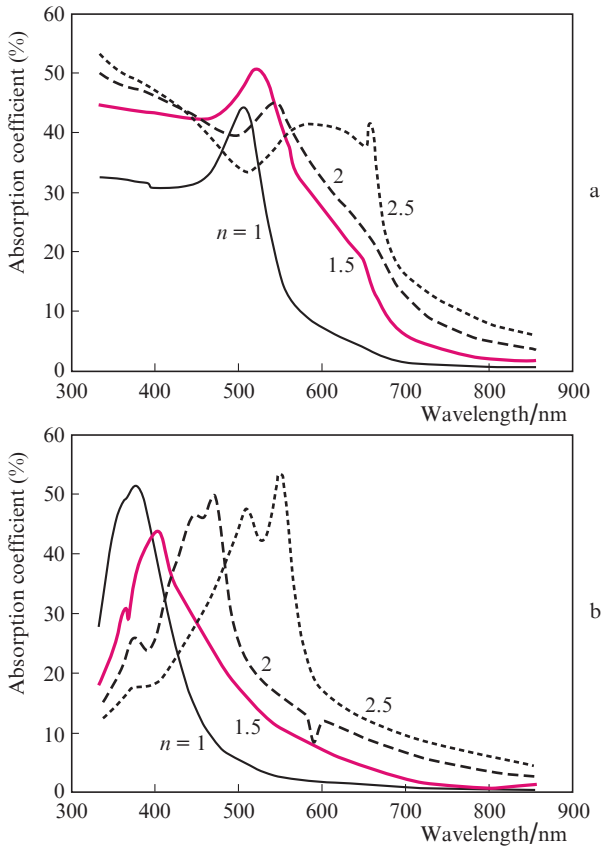

Figure 10. Absorption coefficient vs. wavelength for nanostructures with spherical (a) gold and (b) silver nanoparticles deposited on a fibre end face, calculated for different refractive indices n of the nanoparticle environment.

4. Conclusions

We considered an approach to the computer simulation of the optical properties of nanostructures for fibre-optic photoacoustic converters. The approach makes it possible to establish the physical mechanisms relating the microscopic parameters of nanoparticles and nanostructure with the output characteristics of the entire converter without synthesising test samples. To this end, a method for calculating the light absorption coefficient (which is actually determined by the electromagnetic energy dissipation) based on computation of S-matrices was proposed.

It was found that efficient photoacoustic conversion can be implemented in a surface nanostructure formed by spherical gold nanoparticles on a fibre end face placed in water (in a wide range of the nanostructure microscopic parameters). For example, for the particles with radii of 18–23 nm and the surface occupation density from 35% to 70% does not affect much the conversion performance. Simultaneously, there are three more fairly wide ranges of the parameters, in which high-efficiency photoacoustic conversion can be implemented. For nanostructures with gold or silver nanoparticles on a fibre end face in air, we have a very narrow range of the parameters where all necessary conditions for photoacoustic conversion are satisfied; hence, the applicability of these structures is significantly limited.

It was shown that, in the case of resonance absorption, the back-reflectance is also large; in particular, it is larger than –3 dB at a surface occupation density above 70% for the nanostructure with gold nanoparticles on a fibre end face in air. Hence, when designing photoacoustic generators, one must optically isolate the lasers in use.

References

1. Gang Tingting, Hu Manli, Rong Qiangzhou, Qiao Xueguang, Liang Lei, Liu Nan, Tong Rongxin, Liu Xiaobo, Bian Ce. *Sensors*, **16**, 2125 (2016).
2. Smith R., Arca A., Chen X., Marques L., Clark M., Aylott J., Somekh M. *J. Phys. Conf. Ser.*, **278**, 012035 (2011).
3. Rivero P.J., Goicoechea J., Arregui F.J. *Localized Surface Plasmon Resonance for Optical Fiber-Sensing Applications, Nanoplasmonics – Fundamentals and Applications* (Rijeka: Intech, 2017).
4. Nan Wu, Ye Tian, Xiaotian Zou, Xingwei Wang. *Proc. SPIE*, **8694**, 86940 (2013).
5. Tian Ye, Wu Nan, Zou Xiaontian, Felemban H., Cao Chengyu, Wang Xingwei. *Opt. Eng.*, **52** (6), 065005 (2013).
6. Hou Yang, Kim Jin-Sung, Ashkenazi Shai, Huang Sheng-Wen, Guo L.Jay. *Appl. Phys. Lett.*, **91**, 073507 (2007).
7. Zou Xiaotian, Wu Nan, Tian Ye, Wang Xingwei, Clark M. *J. Acoust. Soc. Am.*, **137** (1), 219 (2015).
8. Belsito L., Vannacci E., Mancarella F., Ferri M., Veronese G.P., Biagi E., Roncaglia A. *J. Micromech. Microeng.*, **24**, 085003 (2014).
9. Hu Chennan, Yu Zhihao, Wang Anbo. *Opt. Express*, **24** (18), 20287 (2016).
10. Zhou Jingcheng, Wu Nan, Bi Siwen, Wang Xingwei. *Proc. SPIE*, **9803**, 98031 (2016).
11. Tian Ye, Wu Nan, Sun Kai, Zou Xiaontian, Wang Xingwei. *J. Comput. Acoust.*, **21** (2), 1350002 (2013).
12. Wu Nan, Tian Ye, Zou Xiaontian, Wang Xingwei. *Proc. SPIE*, **8345**, 83453 (2012).
13. Chen Sung-Liang. *Appl. Sci.*, **7** (25), 1 (2017).
14. Mayeh M., Farahi F. *Phot. Sens.*, **1** (2), 187 (2011).
15. Ortega-Mendoza J.G., Chavez F., Zaca-Moran P., Felipe C., Perez-Sanchez G.F., Beltran-Perez G., Goiz O., Ramos-Garcia R. *Opt. Express*, **21** (5), 6509 (2013).

16. Bishop C.A. *Vacuum Deposition Onto Webs, Films and Foils* (Amsterdam: Elsevier, 2016).
17. Kozadaev K.V. *J. Eng. Phys. Thermophys*., **87** (3), 704 (2014).
18. Kozadaev K.V. *Instrum. Exp. Tech*., **59** (6), 863 (2016).
19. Mikitchuk A.P., Kozadaev K.V. *J. Appl. Spectrosc*., **83** (6), 996 (2017) [*Zh. Prikl. Spektrosk*., **83** (6), 933 (2016)].
20. Goncharov V.K., Kozadaev K.V., Mikitchuk A.P. *High Temp. Mater. Processes: An Intern. Quart. High-Technol. Plasma Processes*, **18** (3), 217 (2014).
21. Kurushin A.A., Plastikov A.N. *Proektirovanie SVCh ustroistv v srede CSTMicrowave Studio* (Design of Microwave Devices in the CST Microwave Studio) (Moscow: Izd-vo MEI, 2010) pp 47–73.
22. Pozar D.M. *Microwave Engineering* (Hoboken: Wiley, 2012).
23. Fritzen F., Bohlke T. *Tech. Mech*., **30** (4), 354 (2010).
24. Golovanov O.A. *Radiotekh. Elektron*., **51** (12), 1423 (2006).
25. Mikitchuk A.P., Kozadaev K.V. *J. Belarus. State Univ. Phys*., **1**, 100 (2017).
26. Dynich R.A., Kovtun-Kuzhel' V.A., Ponyavina A.N. *Zh. Prikl. Spektrosk*., **78** (6), 874 (2012).
27. Goncharov V.K., Kozadaev K.V., Mikitchuk A.P. *Dokl. mezhdunar. nauchnoi konf. 'Aktual'nye problemy fiziki tverdogo tela FTT-2016'* (Proc. Int. Sci. Conf. 'Urgent Problems of Solid-State Physics, FTT-2016') (Minsk: Kovcheg, 2016) Vol. 3.
28. Palik E.D. *Handbook of Optical Constants of Solids* (New York: Academic Press, 1985).
29. Kreibig U., Vollmer M. *Optical Properties of Metal Clusters* (Berlin: Springer-Verlag, 1995).
30. Avramescu A., Lermer T., Muller J., Tautz S., Queren D., Lutgen S., Straub U. *Appl. Phys. Lett*., **95**, 071103 (2009).